Climate Dynamics (2004) 23: 215–227
DOI 10.1007/s00382-004-0435-8

N. Rimbu · G. Lohmann · S. J. Lorenz · J. H. Kim
R. R. Schneider

Holocene climate variability as derived from alkenone sea surface temperature and coupled ocean-atmosphere model experiments

Received: 20 March 2003 / Accepted: 24 March 2004 / Published online: 22 June 2004

Abstract Holocene climate modes are identified by the statistical analysis of reconstructed sea surface temperatures (SSTs) from the tropical and North Atlantic regions. The leading mode of Holocene SST variability in the tropical region indicates a rapid warming from the early to mid Holocene followed by a relatively weak warming during the late Holocene. The dominant mode of the North Atlantic region SST captures the transition from relatively warm (cold) conditions in the eastern North Atlantic and the western Mediterranean Sea (the northern Red Sea) to relatively cold (warm) conditions in these regions from the early to late Holocene. This pattern of Holocene SST variability resembles the signature of the Arctic Oscillation/North Atlantic Oscillation (AO/NAO). The second mode of both tropical and North Atlantic regions captures a warming towards the mid Holocene and a subsequent cooling. The dominant modes of Holocene SST variability emphasize enhanced variability around 2300 and 1000 years. The leading mode of the coupled tropical-North Atlantic Holocene SST variability shows that an increase of tropical SST is accompanied by a decrease of SST in the eastern North Atlantic. An analogy with the instrumental period as well as the analysis of a long-term integration of a coupled ocean-atmosphere general circulation model suggest that the AO/NAO is one dominant mode of climate variability at millennial time scales.

N. Rimbu (✉) · G. Lohmann · J. H. Kim
Bremen University, Department of Geosciences,
PO Box 330400, 28334 Bremen, Germany
E-mail: nrim@palmod.uni-bremen.de

S. J. Lorenz
Max-Planck-Institute for Meteorology,
Model and Data Group, 20146 Hamburg,
Germany

R. R. Schneider
DGO UMR 5805 EPOC, CNRS/Université de Bordeaux I,
33405 Talence, France

G. Lohmann
DFG-Research Center of Ocean Margins, Bremen University,
28344 Bremen, Germany

G. Lohmann
Alfred-Wegner-Institute for Polar and Marine Research,
27570 Bremerhaven, Germany

1 Introduction

The Holocene is the most recent period in the geological record. It began at the time of retreat of the continental ice sheets at the end of the last glaciation, which occurred at about 10 000 calendar years before present (10 cal. kyr BP). Although the Holocene climate appears as relatively stable when viewed in a long-term perspective, significant climate fluctuations were identified during this period (e.g. Bond et al. 1997; Mayewski et al. 1997; deMenocal et al. 2000).

Various terrestrial and marine records show that the Holocene was marked by coherent patterns of climate variability at regional or global scale. These patterns of past climate variability are often related to changes in major phenomena that dominate the last century climate variability like the El Niño Southern Oscillation (ENSO) (Clement et al. 1999; Tudhope et al. 2001; Kitoh and Murakami 2002) or the Arctic Oscillation/North Atlantic Oscillation (AO/NAO) (Rimbu et al. 2003).

We address the question whether the patterns of interannual to decadal variability of the last century climate are relevant for the Holocene climate variability. Our study is focused on the possible role of the AO/NAO in generating global scale climate variability during the Holocene. The signature of the AO/NAO during the Holocene was identified in lacustrine data from the northeastern United States (Noren et al. 2002) as well as in the North Atlantic sediment cores (Keigwin and Pickart 1999). Concordant variations are detected in the time series of sea-salt sodium in the Greenland Ice Sheet Project Two (GISP2) core, believed to be an indicator of

storminess and sea spray in the atmosphere of the high-latitude North Atlantic region (O'Brien et al. 1995; Fisher 2001). In this study, we investigate the dominant modes of tropical and North Atlantic SST variability as well as the coupled variability between these regions during the Holocene.

The work is organized as follows. Data and methods are described in Sect. 2. The spatial and temporal patterns of the SST variability in the tropical and North Atlantic regions as well as the coupled variability of SST from these regions are discussed in Sect. 3. An analogy with the instrumental period is presented in Sect. 4. The interannual to centennial variability in a long-term climate simulation with a coupled ocean-atmosphere circulation model with relevance for Holocene climate variability is presented in Sect. 5. Discussion of the results and the conclusions follow in Sects. 6 and 7, respectively.

2 Data and methods

In this study, we consider 18 SST records solely based on the alkenone method as paleo-thermometry in order to avoid potential bias due to using different SST proxies. The paleotemperature estimates are based on the abundance ratios of long-chain unsaturated alkenones with two to four double bonds (Brassell et al. 1986; Prahl and Wakeham 1987). Alkenones are synthesized by the class *Prymnesionphyceae*of which the coccolithophorids *Emiliania huxleyi* and *Gephyrocapsa oceanica*are the two most common sources of alkenones in contemporary oceans and sediments (Volkman et al. 1980; Conte et al. 1995). Different alkenone unsaturation indices and calibrations were applied for each alkenone SST record (Table 1). The errors in alkenone temperature reported for the culture calibration and for the global core-top calibration reach about 0.5 °C (Prahl and Wakeham 1987) and about 1.5 °C (Müller et al. 1998), respectively. Analytical precision for each record considered here, however, was much better than the one for the calibrations. Detailed core chronologies have been described in previous studies (Table 1). In brief, the age models of SST time series considered in this study were established mainly by accelerator mass spectrometry (AMS) ^{14}C determinations. The age model of the core AD91-17 is additionally based on correlation with oxygen isotopic records (Capotondi et al. 1999; Siani et al. 2001). The mean temporal resolution of each record varies between 64 and 627 years (Table 1).

For the interpretation of the Holocene climate variability that resulted from statistical analysis of alkenone SST data, we looked for an analogous situation in the last century climate. To this purpose we used the sea level pressure (SLP) data set constructed at the Climate Research Unit, at University of East Anglia, UK (Jones 1987) covering the Northern Hemisphere (poleward of 20°N) for the period 1873 to 2000 as well as the global sea surface temperature (SST) data set constructed by Kaplan et al. (1998) for the period 1856 to 2000 for boreal winter (January/February) season.

To better assess the Holocene SST variability, we investigated the interannual to multi-centennial scale variability as resulted from a long-term integration of the ECHO-G ocean-atmosphere coupled model (Legutke and Voss 1999). The ECHO-G consists of the 4th generation atmosphere model ECHAM (T30 horizontal resolution and 19 vertical levels), coupled to the HOPE ocean circulation model, which includes a dynamic-thermodynamic sea-ice model with snow cover (Legutke and Voss 1999). The experiment has a duration of 2300 years of model integration using atmospheric greenhouse gas concentrations (280 ppm CO_2, 700 ppb CH_4, and 265 ppb N_2O) that are typical for the pre-industrial era, and modern solar radiation (Lorenz and Lohmann 2004). The experiment with constant pre-industrial conditions provides a basis for the statistical analysis of long-term spatial and temporal patterns related to natural climate variability.

In our study we used the empirical orthogonal functions (EOF) analysis (von Storch and Zwiers 1999) to provide an objective characterization of the dominant modes of the Holocene SST variability. The eight (ten) well-dated time series of tropical (North Atlantic) SSTs (Figs. 1b and 4b) were reduced into spatially coherent orthogonal eigenvectors. These eigenvectors, together with their corresponding time coefficients (PC) and eigenvalues (a measure of the variance described by each eigenvector) are referred in our study as modes of SST variability. The EOFs also served as a data-filtering procedure to eliminate the noise. A similar procedure was used to identify the dominant mode of Holocene temperature variability in the eastern North Atlantic (Marchal et al. 2002) as well as to analyze the climate variability during the last deglaciation (Clark et al. 2002). We used the EOF analysis also to derive the dominant modes of Northern Hemisphere atmospheric circulation variability at interannual to multi-centennial time scales as resulted from a long-term simulation of the ECHO-G coupled ocean-atmosphere general circulation model.

The dominant modes of coupled tropical-North Atlantic SST variability during the Holocene were identified using a canonical correlation analysis (CCA) (von Storch and Zwiers 1999). The CCA is an appropriate tool to search for linear relationship between two space-time-dependent variables. The CCA selects a pair of spatial patterns of two space-time dependent variables so that their time coefficients are optimally correlated. The time coefficients, or canonical time series, describe the strength and the sign of the corresponding pattern for each realization in time. Prior to the CCA, the original data were projected onto their EOFs and only a limited number of them were retained, explaining most of the total variance.

The temporal patterns of the time coefficients of the dominant EOFs of alkenone SST variability were

Table 1 Description of the cores analyzed in this study

No.	Core name	Lat.	Long.	Water depth (m)	Dating	^{14}C dating no. used for age model	Mean sample interval (min.-max.) (cm)	Mean time resolution (min.-max.) (yr)	Alkenone index	Alkenone calibration	Reproducibility (°C)	Reference
Tropics												
1	M35003-4	12.083	-61.250	1299	AMS ^{14}C	5	5	~264 (152-297)	UK'37	Müller et al. 1998	0.3 ($\pm 1\sigma$)	Rühlemann et al. 1999
2	ODP 658C	20.750	-18.583	2262.9	AMS ^{14}C	8	~2 (1-11)	~101 (27-370)	UK'37	Prahl et al. 1988	-	Zhao et al. 1995; deMenocal et al. 2000
3	ODP 1078C	-11.920	13.400	426	AMS ^{14}C	7	10	~242 (82-386)	UK'37	Müller et al. 1998	0.1 ($\pm 1\sigma$)	Kim et al. 2003
4	MD79257	-20.400	36.333	1262	AMS ^{14}C	4	~11 (4-60)	~297 (100-1700)	UK'37	Prahl et al. 1988	0.3 ($\pm 1\sigma$)	Duplessy et al. 1991; Bard et al. 1997; Sonzogni et al. 1998
5	74KL	14.321	57.347	3212	AMS ^{14}C	5	~3 (2.5-5)	~278 (182-722)	UK'37	Prahl et al. 1988	0.2 ($\pm 1\sigma$)	Sirocko et al. 1993; Kim et al. 2004
6	18287-3	5.650	110.650	598	AMS ^{14}C	3	~10 (5-10)	~327 (103-725)	UK'37	Pelejero and Grimalt 1997	0.2 ($\pm 1\sigma$)	Kienast et al. 2001
7	17964	6.158	112.213	1556	AMS ^{14}C	4	~19 (9-20)	~627 (420-784)	UK'37	Müller et al. 1998	0.15 ($\pm 1\sigma$)	Pelejero et al. 1999a, 1999b; Wang et al. 1999
8	17940-2	20.117	117.383	1727	AMS ^{14}C	12	~8 (2-13)	~143 (23-275)	UK'37	Müller et al. 1998	0.15 ($\pm 1\sigma$)	Pelejero et al. 1999a; Wang et al. 1999
North Atlantic Realm												
9	SU81-18	37.767	-10.183	3135	AMS ^{14}C	8	~7 (3-11)	~525 (180-837)	UK'37	Prahl et al. 1988	0.3	Bard et al. 2000
10	M39-008	36.382	-7.077	576	AMS ^{14}C	7	~5 (5-10)	~137 (15-1265)	UK'37	Müller et al. 1998	0.15 ($\pm 1\sigma$)	Cacho et al. 2001
11	MD952043	36.143	-2.622	1841	AMS ^{14}C	8	~5 (2-10)	~121 (34-223)	UK'37	Müller et al. 1998	0.15 ($\pm 1\sigma$)	Cacho et al. 1999
12	IOW225517	57.667	7.091	293	AMS ^{14}C	7	~5 (1-10)	~111 (18-224)	UK'37	Müller et al. 1998	-	Emeis et al. 2003
13	MD952011	66.967	7.633	1048	AMS ^{14}C	10	~4 (1-15)	~64 (4-266)	UK'37	Prahl and Wakeham 1987	0.15 ($\pm 1\sigma$)	Calvo et al. 2002
14	IOW225514	57.838	8.704	420	AMS ^{14}C	6	~5 (1-5)	~77 (8-271)	UK'37	Müller et al. 1998	-	Emeis et al. 2003
15	M23258-2	74.995	13.970	1768	AMS ^{14}C	10	~4 (2-6)	~193 (119-349)	UK'37	Rosell-Melé et al. 1995	-	Marchal et al. 2002; Sarnthein et al. 2003
16	RL11	36.746	17.718	3376	AMS ^{14}C	3	~1 (1-3)	~259 (105-804)	UK'37	Müller et al. 1998	-	Emeis et al. 2000
17	AD91-17	40.870	18.636	844	AMS ^{14}C, isotope stratigraphy	5	~4 (2-6)	~158 (45-442)	UK'37	Müller et al. 1998	-	Giunta et al. 2001
18	GeoB 5844-2	27.714	34.682	963	AMS ^{14}C	6	~2 (1-3)	~295 (151-453)	UK'37	Prahl et al. 1988	0.6 ($\pm 1\sigma$)	Arz et al. 2003

UK′37 = C37:2/(C37:2 + C37:3) according to Prahl and Wakeham (1987)
UK37 = (C37:2-C37:4)/(C37:2 + C37:3 + C37:4) according to Brassell et al. (1986)
Prahl and Wakeham (1987): T(°C) = (UK37 + 0.11)/0.04
Müller et al. (1998): T (°C) = (UK′37–0.044)/0.033
Pelejero and Grimalt (1997): T(°C) = (UK′37–0.092)/0.031
Rosell-Melé et al. (1995): T(°C) = (UK37-0.093)/0.03

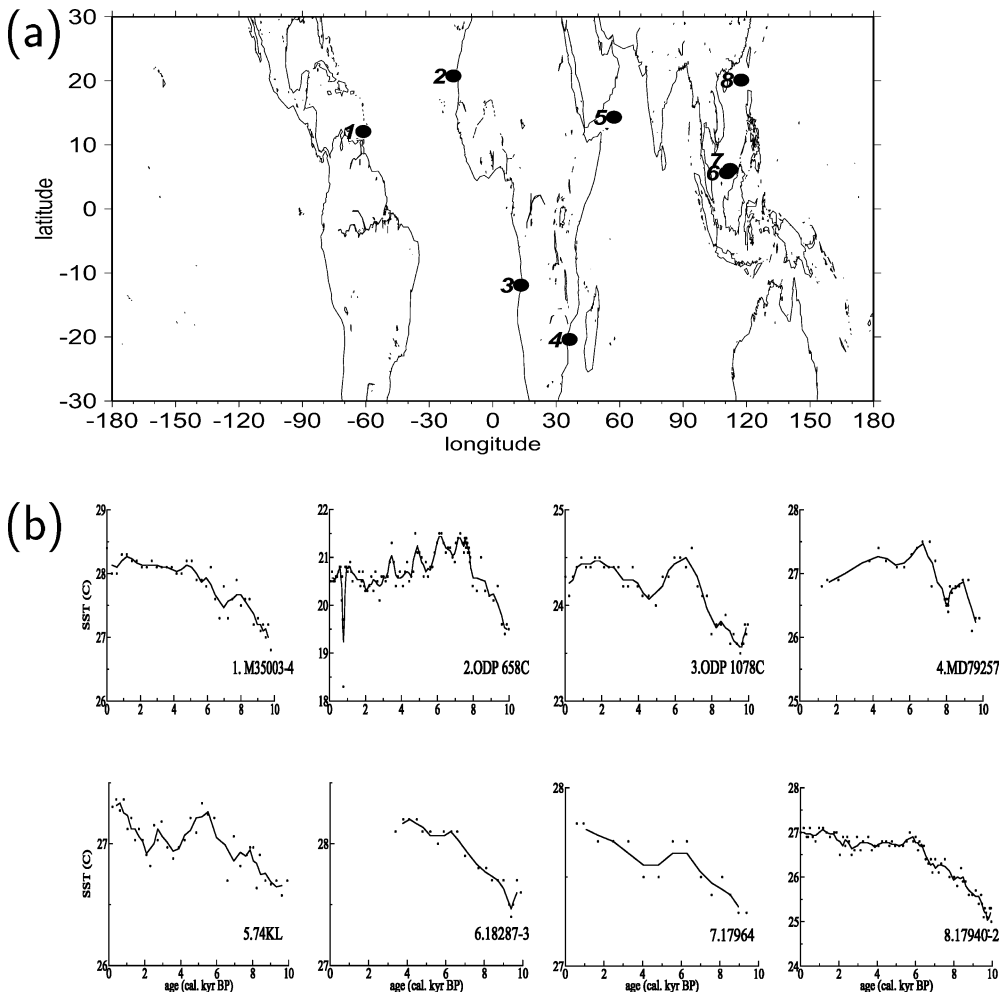

Fig. 1 **a** Marine sediment core positions from the tropical region (25°S to 25°N) analyzed in this work. **b** Original SST (*dotted*) and the 3-point smoothed (*solid*) time series from the tropical region used in this study. The *names* of the cores are indicated in the *lower right corner* of each panel. All SST records are based on the alkenone method

investigated using the singular spectrum analysis (SSA, Ghil et al. 2002). The SSA is designed to decompose a short and noisy time series into three statistically independent components: trends, oscillatory patterns and noise. The trends need not to be linear and the oscillations can be amplitude and phase modulated (Ghil et al. 2002). In our analysis all time components with a time scale longer than 3 kyr (i.e. the size of the window) are referred as trends while the time components with time scales smaller than 3 kyr are referred as centennial to millennial scale variations. To filter out the noise, we reconstructed the centennial to millennial scale signal from several SSA components (usually four) and analyzed this reconstructed signal using the multi taper method (MTM, Ghil et al. 2002).

These statistical methods require that the SST values from the different records are available for the same time intervals. SST values in 100 years time intervals were derived using linear interpolation. The SST anomalies against the SST mean over the considered period were calculated for each record and normalized with the corresponding temporal standard deviation. Prior to statistical analysis, the SST time series were smoothed with a 300 year running mean filter.

3 Tropical and North Atlantic Holocene variability from alkenone SST data

3.1 Tropical SST variability

The alkenone SST records from the tropical region (Fig. 1a) show a general increase in the SST from the early to late Holocene (Fig. 1b). Superimposed on this positive trend, a long-term SST variation with a maximum around 4–7 cal. kyr BP is seen in most of the time series. These SST reconstructions also show important fluctuations at centennial to millennial time scales (Fig. 1b).

To better assess the long-term variability of tropical SST during the Holocene, we analyzed the time series represented in Fig. 1b with the EOF method. The first EOF (Fig. 2a), which describes 67% of the variance, has a monopolar structure. Its associated time coefficients (PC1) indicate a variable positive trend (Fig. 2b). This mode captures a rapid increase in tropical SST from the beginning of the Holocene at about 10 cal. kyr BP to about 6 cal. kyr BP as well as a moderate warming from 6 cal. kyr BP to the present. Small amplitude fluctuations at centennial to millennial time

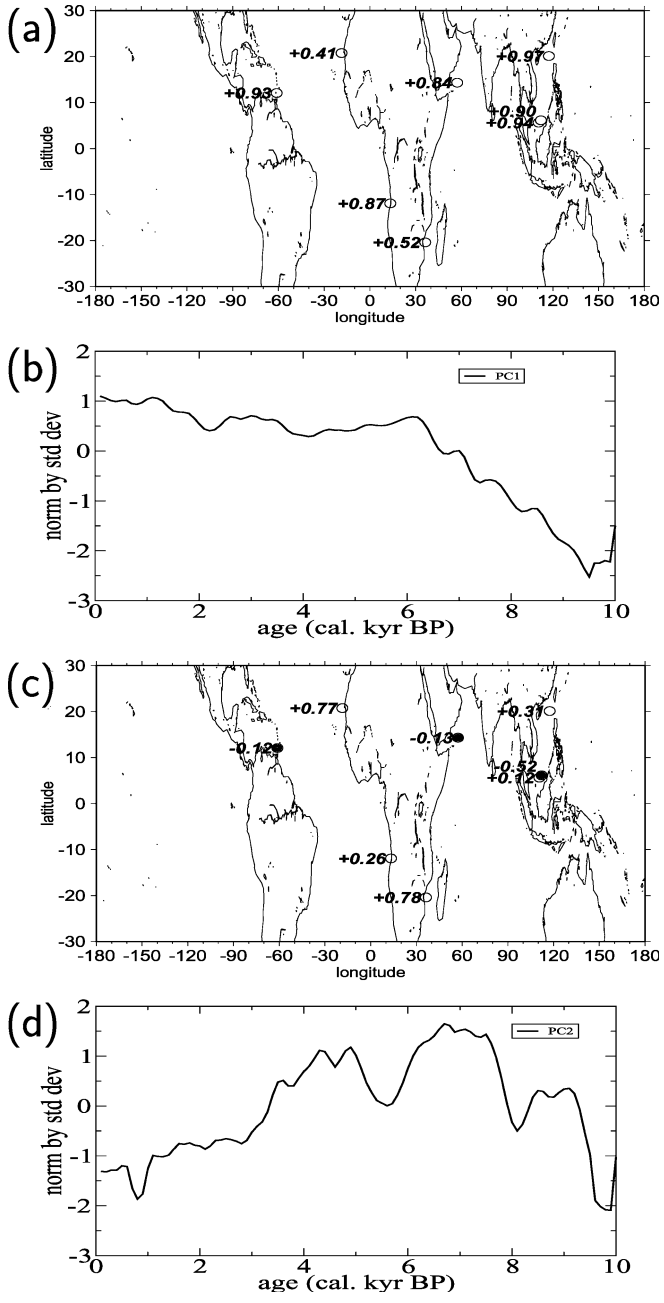

Fig. 2 **a** The first EOF of tropical SST variability during the Holocene. **b** The associated time coefficients. **c** and **d**, as in **a** and **b**but for the second EOF. The values from the EOF maps are the correlation coefficients between the corresponding time coefficients and the normalized SST field

scales are superimposed on these long-term trends (Fig. 2b).

The second EOF of the SST data from this region describes 19% of the variance (Fig. 2c). The time coefficients of this mode (PC2) show a maximum around 4–7 cal. kyr BP (Fig. 2d). This indicates a relative high SST during this period in the northern and southern part of the tropical region as defined in our study. This tendency can be directly detected through a visual inspection of the records 2 (ODP 658C), 3 (ODP 1078C), 4 (MD79257) and 8 (17940-2) shown in Fig. 1b. The PC2 shows also centennial to millennial scale fluctuations (Fig. 2d).

In order to identify the temporal patterns of tropical SST variability during the Holocene, we decomposed the time coefficients associated to the leading modes of SST variability from this region (Fig. 2b, d) using SSA. The reconstructed signal from the first two SSA components (i.e. trends) of the PC1, which describes 94% of the variance, captures the long-term transition of the tropics from relatively cold conditions during the early Holocene to relatively warm conditions during the late Holocene (Fig. 3a). The reconstructed signal from the next four SSA components, which describes 4% of the variance, shows enhanced millennial scale variability (Fig. 3b). The MTM spectrum of this signal (Fig. 3c) reveals significant peaks around 2.3 and 0.7 kyr. The trend pattern of the PC2 as resulted from the SSA shows a maximum around 4–7 cal. kyr BP (Fig. 3d). The MTM spectrum of the PC2 variations in the centennial to millennial band (Fig. 3e) shows a significant peak around 2.3 kyr (Fig. 3f).

3.2 North Atlantic SST variability

The SST records from the North Atlantic region (Fig. 4a) indicate both positive and negative trends as well as important centennial to millennial scale variations (Fig. 4b). The records from the eastern North Atlantic and from the western Mediterranean Sea indicate a general cooling from the early to late Holocene, consistent with a previous study (Marchal et al. 2002). The record 18 (GeoB5844-2) from the northern Red Sea indicates a general warming from the early to the late Holocene. A moderate warming is indicated also by the core 16 (RL11) from the central Mediterranean Sea (Fig. 4b). Superimposed on these trends, some records show relatively high temperature values around 4–7 cal. kyr BP, similar to the tropical records (Fig. 1b). Consistent with this visual observation, the first EOF of SST records from this region (Fig. 5a), which describes 60% of the SST variance, emphasizes an out of phase relationship of SST variations from the eastern North Atlantic as well as the western Mediterranean Sea and the northern Red Sea. This Holocene SST pattern resembles the AO/NAO SST related pattern in this region during the last century (e.g. Hurrell et al. 2003). This mode captures the transition from relatively cold (warm) conditions in the northern Red Sea (the eastern North Atlantic and the western Mediterranean Sea) during the early Holocene to relatively warm (cold) conditions in these regions during the late Holocene. A similar pattern was identified in this region based on twelve alkenone time series of different resolution (Rimbu et al. 2003). The second EOF of the SST reconstruction from this region (Fig. 5c) describes 18% of the SST variance. Its time coefficients (Fig. 5d) show a maximum around 4–7 cal. kyr BP. This indicates rel-

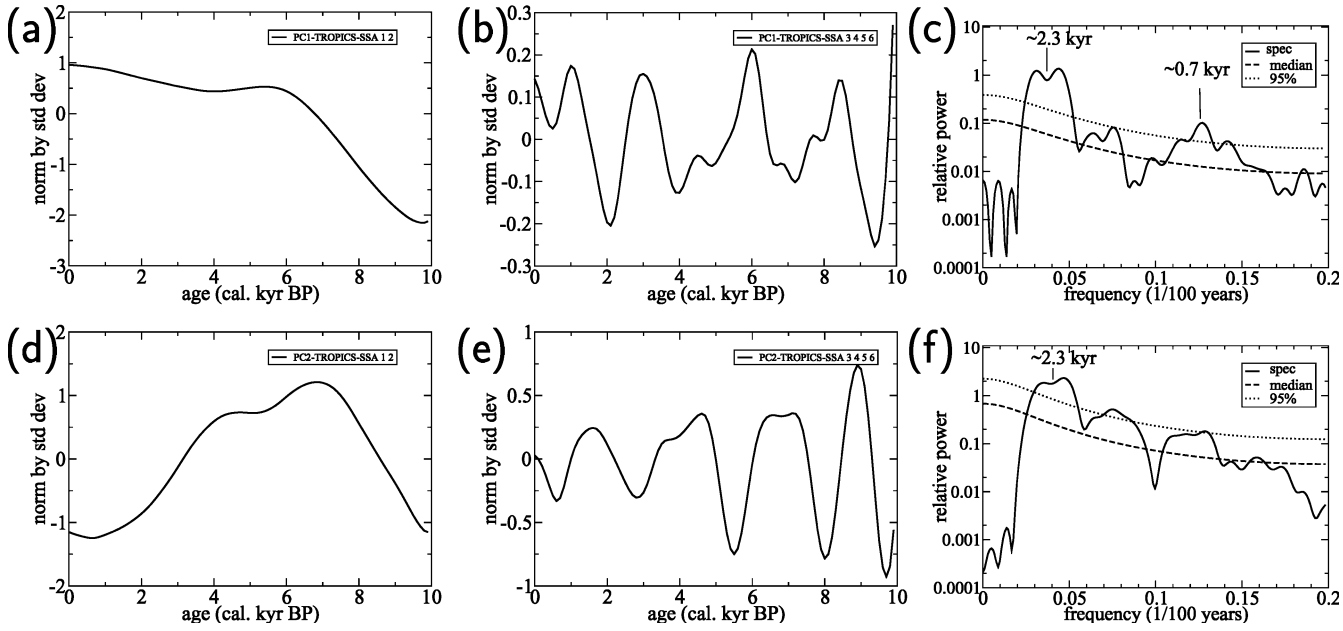

Fig. 3 Reconstruction of the time coefficients of the first EOF of the tropical SST variability from **a** the first two SSA components (i.e. trends) and **b** from the next four SSA components. **c** The MTM spectrum of the time series represented in **b**. Median noise background and 95% confidence level relative to the null hyphothezis of first order autoregressive 'red noise' process are shown. **d**–**f**, as in **a**–**c** but for the second EOF

atively warm conditions during this period over most parts of the North Atlantic region.

Similar to the tropics, we decomposed the time coefficients of the two leading modes of North Atlantic region SST variability during the Holocene in trends and centennial to millennial scale variations using the SSA. The trend signal, which describes 96% of the PC1 variance, shows weak variations from 10 cal. kyr BP to about 6 cal. kyr BP followed by a strong increase with a maximum around 1–2 cal. kyr BP. The reconstructed signal from the next four SSA components, describing 3% of the variance (Fig. 6b), shows enhanced centennial scale variability. The MTM spectrum of this signal (Fig. 6c) shows two peaks around 2.3 and 1 kyr. As for the tropics, the SSA decomposition of the PC2 shows a trend pattern with a maximum around 4–7 cal. kyr BP. The reconstructed signal in the centennial to millennial band (Fig. 6e) emphasizes enhanced variability around 2.3 kyr (Fig. 6f).

3.3 Coupled tropical-North Atlantic SST variability

The EOF analysis of the tropical and North Atlantic SST variability during the Holocene reveals that a warming in the northern Red Sea as well as a cooling in the eastern North Atlantic and the western Mediterranean Sea is accompanied by a warming over the entire tropical region. Furthermore, the 2.3 kyr cycle seems to be a common characteristic of both the tropical and North Atlantic regions. In order to better assess this relationship, we perform a CCA analysis of the alkenone SST records from the tropical and North Atlantic regions.

The leading CCA mode of tropical SST (Fig. 7a) explains 37% of the variance. This mode shows in phase variations of the SST at six core locations. Only the cores 2 (ODP 658C) and 4 (MD79257) show SST variations of the opposite sign (Fig. 2a). The leading CCA mode of SST variability from the North Atlantic region (Fig. 7b) resembles the SST anomaly pattern associated with the AO/NAO during the last century (e.g. Hurrell et al. 2003). This pattern describes about 64% of the alkenone SST variance. The corresponding time coefficients (Fig. 7c) show variations similar to those of time coefficients of the first EOF of the North Atlantic SST variability (Fig. 5b). In brief, the CCA indicates that a decrease (increase) in the eastern North Atlantic (the northern Red Sea) SST is associated with an increase in SST in the tropical region. This pattern of SST variability can be detected also directly through a visual inspection of the alkenone SST records from the tropical (Fig. 1b) and North Atlantic (Fig. 4b) regions.

4 Analogy with the instrumental period

In order to evaluate the nature of climatic connections between the tropical and North Atlantic regions during the Holocene, an analogous situation in the last century climate is examined. For this purpose, we investigated the relationship between the dominant mode of Northern Hemisphere atmospheric circulation and global SST for the period 1873 to 2000. Prior to the EOF analysis, the winter (DJF) SLP data were detrended and normalized with the local standard deviation. All time scales from interannual to multi-decadal were considered in our EOF analysis.

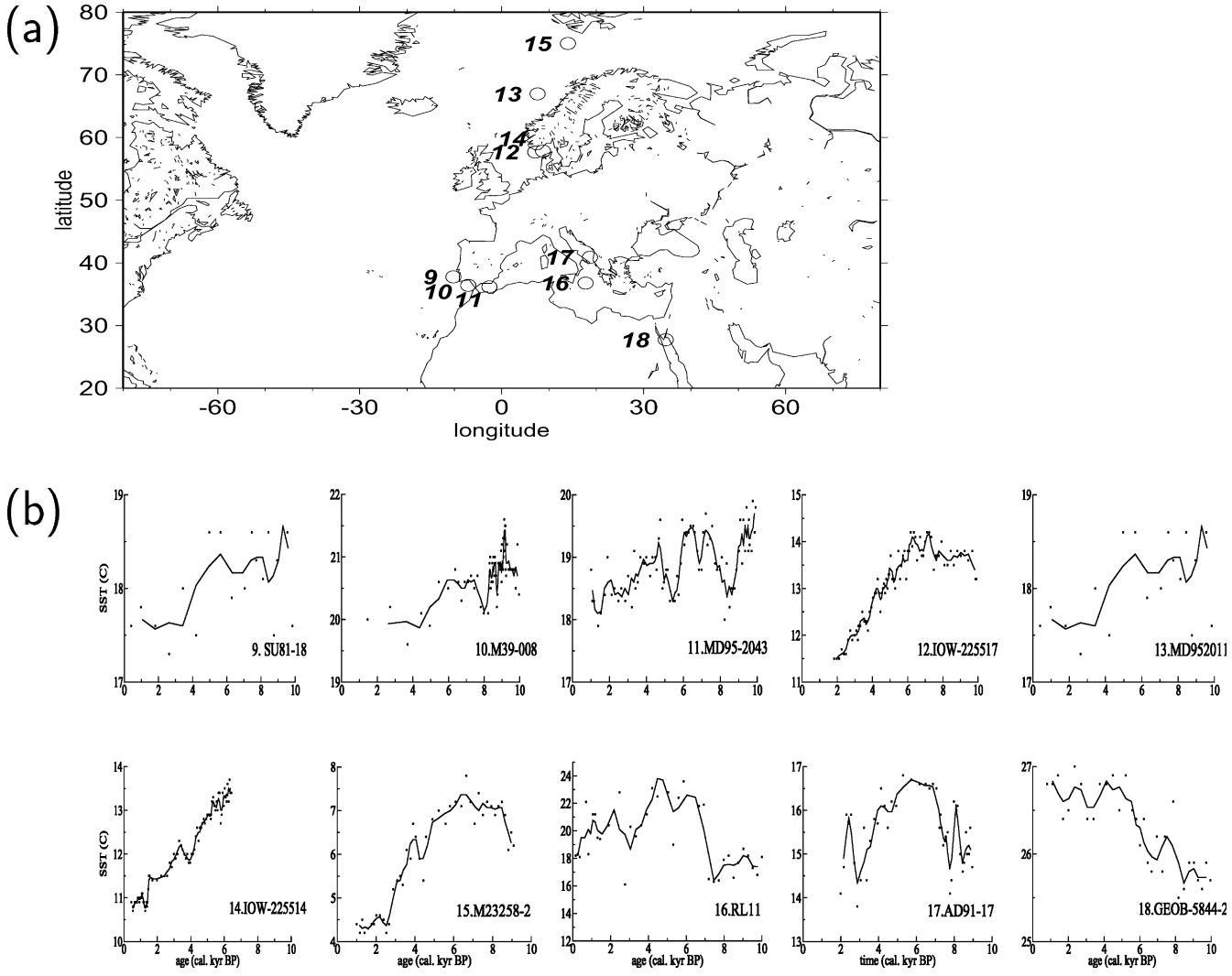

Fig. 4 **a** Marine sediment core positions from the North Atlantic realm analyzed in this work. **b** Original SST (*dotted*) and the 3-point smoothed (*solid*) time series from the North Atlantic realm used. The *names* of the cores are indicated in the *lower right corner* of each panel. All SST records are based on the alkenone method

The first EOF of the Northern Hemisphere winter SLP variability has an annular structure with an out-of-phase relationship between the polar and midlatitude regions (Fig. 8a). This pattern resembles the AO/NAO (Thompson and Wallace 1998). Globally, it explains 22% of the SLP variance. The correlation map of the time coefficients of this pattern (PC1) and global SST (Fig. 8b) shows significant (95% level) negative correlations over the tropical Atlantic and some regions of tropical Pacific and Indian oceans as well as significant positive (negative) correlations in the eastern North Atlantic (the northern Red Sea). Therefore, enhanced negative SST anomalies in the tropical region together with positive (negative) SST anomalies in the eastern North Atlantic (the eastern Mediterranean Sea and the northern Red Sea) may be an indication of an enhanced positive phase of the AO/NAO at these time scales. Consistent with these results, negative SST anomalies in the tropical Pacific (i.e. La Niña conditions) are statistically significantly related to a SLP pattern in the North Atlantic similar to the positive phase of NAO when the entire observational period is considered in the analysis (Pozo-Vázquez et al. 2001).

The tropical and North Atlantic SST patterns as derived from CCA (Fig. 7) indicate that positive (negative) SST anomalies in the eastern North Atlantic (the northern Red Sea) are associated with negative SST anomalies in the tropical region. This pattern of the global Holocene SST variability is qualitatively similar to the SST pattern associated to the AO/NAO during the last century (Fig. 8b). This suggests a possible role of AO/NAO in generating the Holocene SST variability.

5 Coupled ocean-atmosphere general circulation model experiment

To better relate the centennial to millennial scale Holocene variability resulting from the statistical analysis of alkenone SST data with natural climate

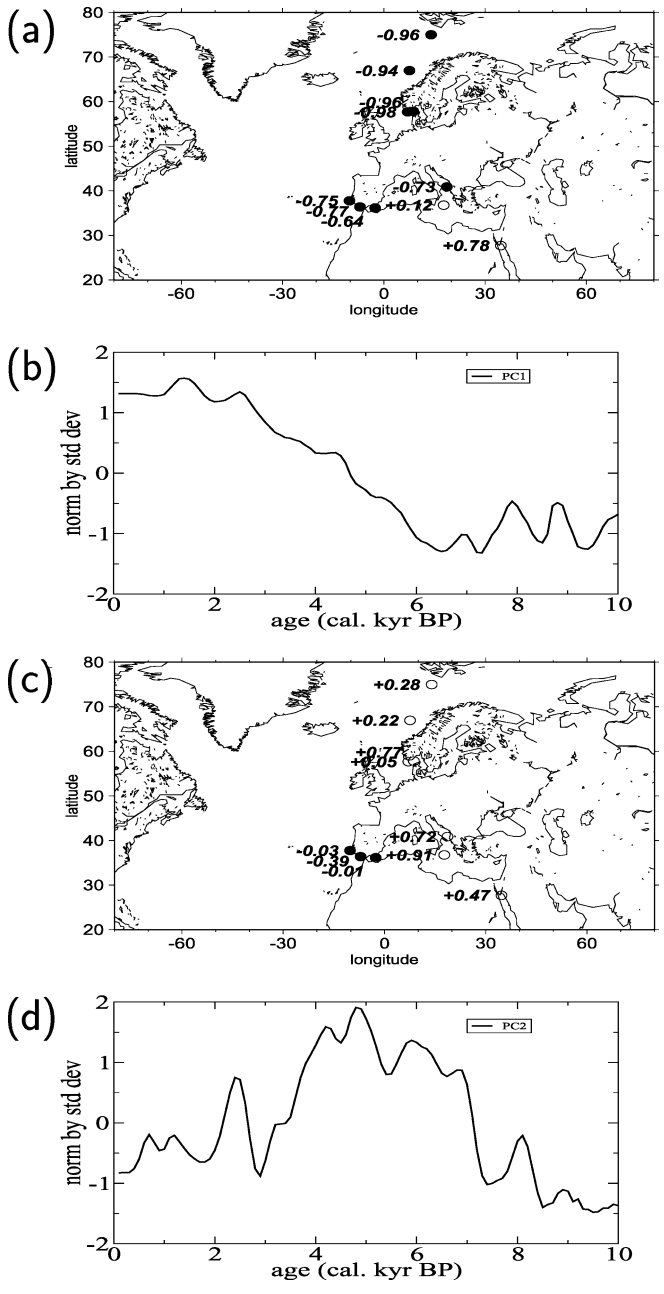

Fig. 5 **a** The first EOF of the North Atlantic SST variability during the Holocene. **b** The associated time coefficients. **c** and **d**, as in **a**, **b** but for the second EOF. The values from the EOF maps are the correlation coefficients between the corresponding time coefficients and the normalized SST field

variability, we analyzed the data from a long-term integration of the ECHO-G coupled model. Details of these climate simulations are given by Lorenz and Lohmann (2004). It should be noted that in this climate simulation the variability is generated only by internal processes while the alkenone SST variability and the variability during the instrumental period are due to both internal and external forcing.

We compared the model simulation with instrumental data investigating the relation between the dominant mode of the Northern Hemisphere atmospheric circulation and the global surface temperature for interannual to multi-decadal time scales. Prior to the EOF analysis, we filtered the simulated data in the 1–100 year frequency band, in order to retain these time scales, only. The first EOF of the Northern Hemisphere SLP variability at these time scales as simulated with this model (Fig. 9a) describes 30% of the SLP variance. It has an annular structure similar to the AO/NAO pattern derived from instrumental data (Fig. 8a). The temperature pattern associated to this simulated pattern is very similar to the corresponding pattern based on instrumental data from 1873 to 2000 period (Fig. 8b).

For multi-centennial time scales (i.e. time scales longer than 100 years), the first EOF of Northern Hemisphere SLP variability, which describes 40% of the SLP variability in the model simulation, also has an annular structure (Fig. 9c). The correlation map of the time coefficients of this EOF with simulated surface temperature (Fig. 9d) shows a pattern that is qualitatively similar to the corresponding temperature pattern from interannual to multi-decadal time scales (Fig. 9b).

6 Discussion

The statistical analysis of our alkenone SST data reveals that during the early Holocene relatively high (low) SST in the eastern North Atlantic (the northern Red Sea) was accompanied by relatively low SST (i.e. La Niña like conditions) in the tropical region. Consistent with the indications shown by our alkenone SST data, Ecuadorian varved lake sediments (Rodbell et al. 1999) and corals from Papua New Guinea (Tudhope et al. 2001) indicate that ENSO events were considerably weaker between 8.8 and 5.8 cal. kyr BP. Predominant La Niña conditions in the tropical Pacific during the early Holocene are suggested also by model simulations. A simulation with an intermediate complexity ENSO model (Zebiak and Cane 1987) forced by variations in heating due to orbital variations in seasonal insolation shows weaker ENSO activity in the early to mid Holocene than in the late Holocene (Clement et al. 1999). Another recent model simulation shows that tropical Pacific temperature and circulation patterns at 6 cal. kyr BP are similar to those observed at the present-day La Niña period (Kitoh and Murakami 2002). Based on an analogy with instrumental period as well as on the results of our model simulation, we argue that this early to mid Holocene temperature pattern is compatible with an enhanced positive phase of AO/NAO during this period.

The first EOF of Northern Hemisphere winter SLP for the period 1873 to 2000 has an annular structure. The correlation map of the time coefficients of this EOF and SST over this period indicates significant negative (positive) correlations over most parts of the tropical region, the eastern Mediterranean Sea and the northern

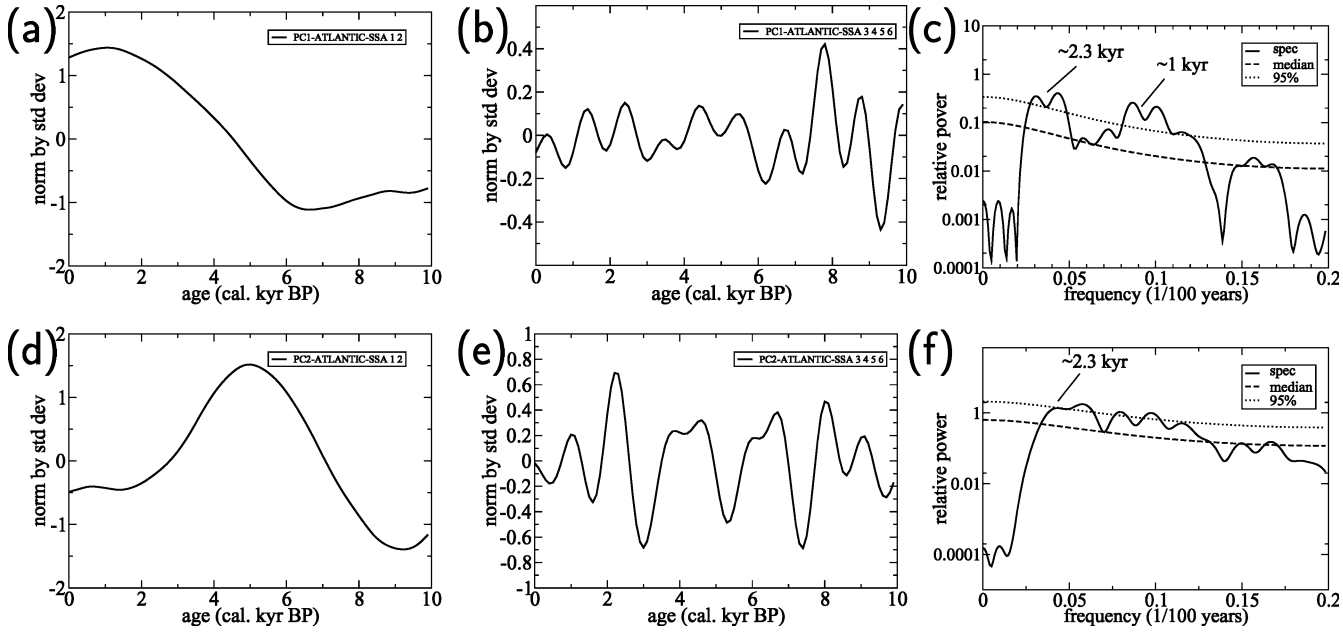

Fig. 6a–f Same as in in Fig. 3, but for the North Atlantic SST variability

Red Sea (the eastern North Atlantic). A similar relationship is suggested for the instrumental period (e.g. Pozo-Vázquez et al. 2001). The dominant patterns of Holocene alkenone based SST reconstructions from the tropical and North Atlantic regions are similar to the SST patterns associated with the AO/NAO SST related pattern during the 1873 to 2000 period. This suggests a possible role of the AO/NAO in generating the trend SST pattern as captured by the first CCA modes of tropical and North Atlantic alkenone SST data.

The second EOF of SST from tropical and North Atlantic regions suggest a relatively warm period around 4–7 cal. kyr BP period. This warming period is also reflected in other proxy records from many parts of the world, although the dating of the climatic episode is variable and there are geographical differences in the timing of the thermal maximum (e.g. Marchal et al. 2002). This mode captures also the relatively cool periods at the beginning and end of the Holocene.

Our coupled model simulation indicates basically the same temperature pattern associated with the simulated AO/NAO for time scales ranging from interannual to multi-centennial. This suggests that the AO/NAO plays an important role in generating not only trends but also millennial scale variability during the Holocene. The dominant modes of tropical and North Atlantic Holocene SST emphasize enhanced variability around 2.3 kyr. A cycle of about 2.5 kyr also characterizes glacier advances in Europe, North America, New Zealand (Denton and Karlen 1973) and central Asia (Zhang et al. 2000). Furthermore, a 2.5 kyr cycle is seen in the Indian Ocean hydrography (Pestiaux et al. 1988). The latter has been attributed to a combination tones of the orbital precessional and obliquity cycles,

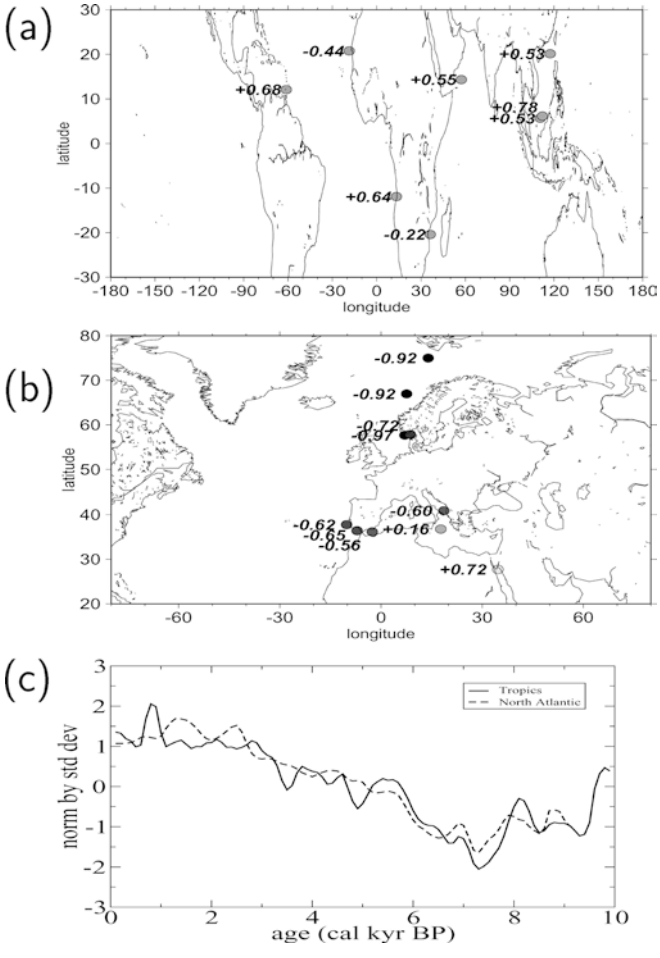

Fig. 7 Leading CCA modes of the Holocene SST variability in **a** the tropics and **b** the North Atlantic realm. **c** The corresponding time coefficients

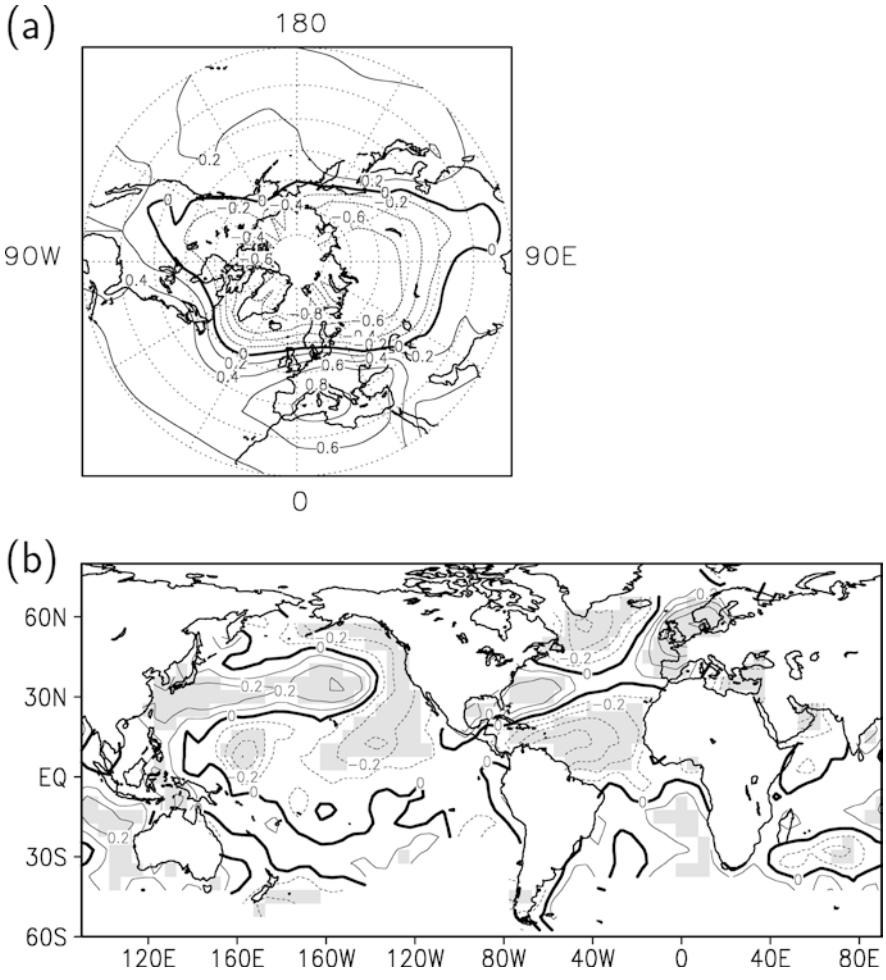

Fig. 8 **a** The first EOF of Northern Hemisphere winter SLP variability for the period 1873–2000. **b** The correlation map of time coefficients of the SLP pattern represented in **a** and global sea surface temperature for the period 1873 to 2000. *Shading* indicates local statistical significance of the correlations at 95% confidence level based on a *t*-test. Data were detrended and normalized prior to the analysis

representing an internal nonlinear response of the monsoon system to solar forcing (Hagelberg et al. 1994). The alkenone-based SST patterns suggest that the 2.3 kyr cycle is linked to the strength of AO/NAO during the Holocene. This is consistent with the results reported by Rohling et al. (2002), who showed that increasing in the strength, duration and frequency of northerly polar continental air outbreaks over the Aegean Sea follows a 2.3 kyr cycle modulating the temperature in this region. Indeed, the enhanced northerly advection of continental air over the Agean Sea is the regional manifestation of AO/NAO bringing cold air from Southern Europe over the eastern Mediterranean Sea during its positive phase (Rimbu et al. 2001). In the multi-centennial band, the time coefficients of the dominant pattern of North Atlantic SST variability show enhanced variability at about 1 kyr. This cycle also characterizes the Holocene isotope data from the GISP2 ice core (Grootes and Stuiver 1997) as well as various reconstructed climate variables from Northern and Central Europe (Schulz and Paul 2002). The time coefficients of the first EOF in the tropical region also show enhanced variability in the multi-centennial band at about 0.7 kyr. A similar cycle characterizes the East Asian monsoon regime (Wang et al. 1999).

The AO/NAO variability at different time scales can be linked to both internal and external forcing. Model studies have shown that significant variability at time scales ranging from interannual to multi-centennial can be generated by atmospheric processes (James and James 1989; Garric and Huber 2003), oceanic or coupled ocean-atmosphere system (Latif and Barnett 1994; Goodman and Marshall 1999; Delworth and Mann 2000) and sea-ice system. All these internal processes could partly generate the AO/NAO variability shown by our model simulation. External forcing, like volcanic activity or solar irradiance (Shindell et al. 2001, 2003) could also be related to long-term variability of the AO/NAO. Further studies will clarify wheather the AO/NAO Holocene variability as suggested by the SST alkenone records considered in this study is related to internal or external forcing.

7 Conclusions

The analysis of alkenone-based SST reconstructions, an analogy with the instrumental period as well as a long-term simulation of the coupled ocean-atmosphere ECHO-G model suggest an important role of the AO/

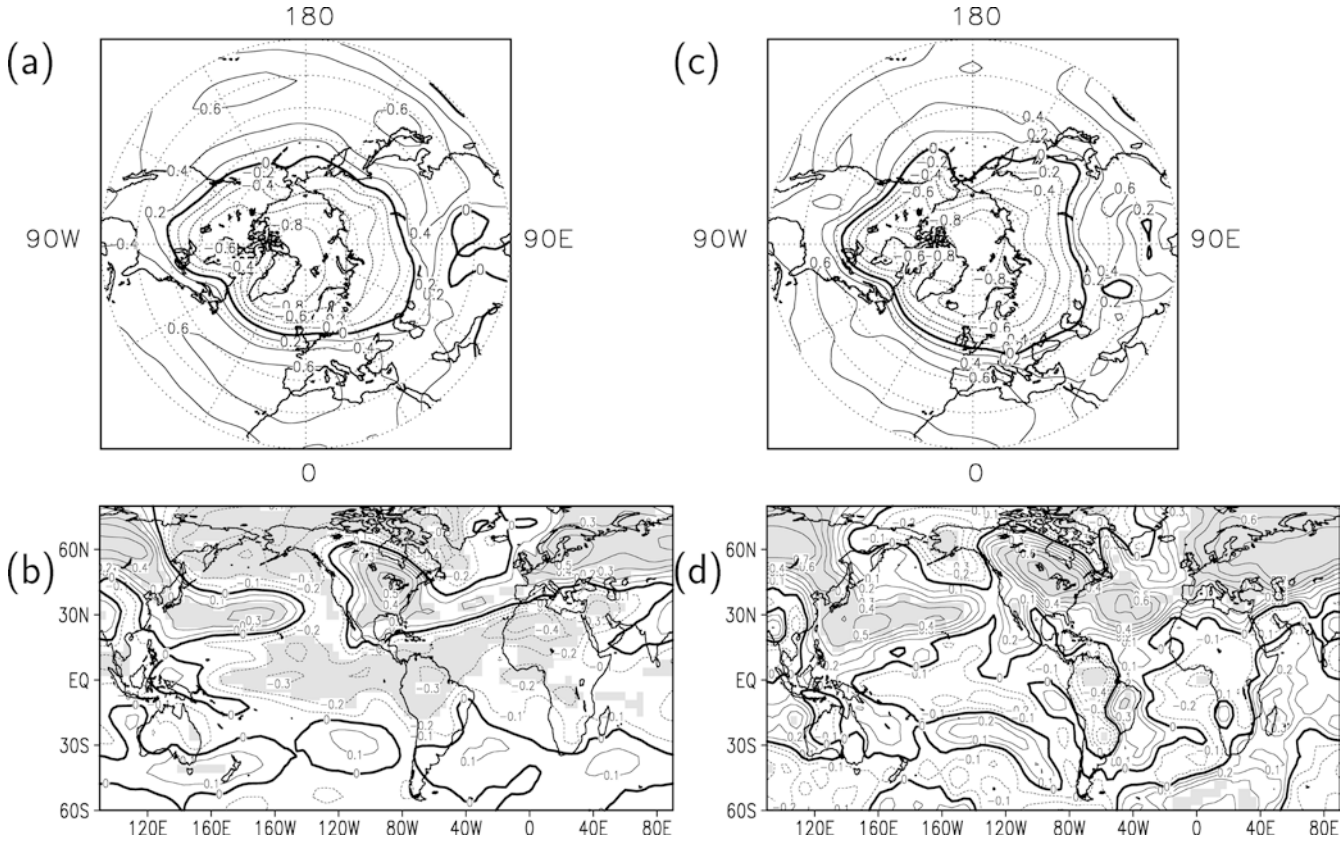

Fig. 9 **a** The first EOF of interannual to multi-decadal SLP variations from a long-term simulation with the ECHO-G coupled ocean-atmosphere general circulation model. **b** The correlation map of the time coefficients of the SLP pattern represented in **a** with simulated global surface temperature. *Shading* indicates local statistical significance of the correlations at 95% confidence level based on a *t*-test. **c**, **d**, as in **a**, **b** but for multi-centennial time scales. Prior to the analysis the data were filtered in the interannual to decadal band (1–100 year) and multi-centennial band (greater than 100 years), respectively

NAO in generating trends as well as centennial to millennial scale SST variability during the Holocene. A large part of the trend in AO/NAO during the Holocene as suggested by the alkenone data is most likely related to Milankovitch forcing. Recent modelling experiments reveal that changes in the regional circulation in the Nordic Seas during the Holocene is compatible with Milankovitch forcing (Lohmann et al. 2004). A recent model simulation (Rimbu et al. 2003) shows that the enhanced positive phase of the AO/NAO at 6 cal. kyr BP relative to present-day is accompanied by relatively low insolation in the tropical region. In this simulation the transition from more positive to more negative phase of AO/NAO from 6 cal. kyr BP to the present-day is related to the increase of tropical insolation during the winter season associated with the Earth's precession at cycle. The second modes of Holocene SST variability from the tropical and North Atlantic regions describe the relatively high temperature pattern during 4–7 cal. kyr BP. This warm period is also observed for temperature reconstructions derived from terrestrial vegetation (Huntley and Prentice 1988) and mountain glaciers (Porter and Orombelli 1985), and is often referred to as the Holocene Climatic Optimum (Crowley and North 1991).

The leading modes of alkenone-based Holocene SST investigated in our study show enhanced variability at a time scale of about 2.3 kyr. We showed that this cycle, which was detected in various particular paleorecords (Bond et al. 1997; Mayewski et al. 1997; Rohling et al. 2002) has a global character. The global scale of this mode may be related not only to a global forcing (e.g., Rohling et al. 2002) but also to tropical-extratropical atmospheric teleconnections as shown here.

The statistical analysis of our alkenone SST data set as well as the model simulation show consistent patterns of Holocene climate variability. However, we should keep in mind that the Holocene patterns shown in this work are based on a low spatial and temporal resolution SST data set. In particular, the period and amplitude of cyclicities identified in the multi-centennial band are subject to large errors. Also the alkenone SST data can suffer from bias due to influence of environmental parameters other than temperature (Bard 2001). Therefore, additional high resolution spatio-temporal proxy data sets are necessary to examine the spatial and temporal patterns of Holocene climate variability. Model experiments with different forcing factors will be performed in order to establish the physical mechanisms behind the dominant modes of Holocene climate variability.

Acknowledgements We would like to thank I. Cacho, J. Grimalt and K.-C. Emeis for providing their alkenone data as GHOST contributors (http://www.Pangaea/Projects/GHOST). This study was funded by grants from the German Ministry of Research and Education (BMBF) through the program DEKLIM. We thank the reviewers for their constructive comments. RCOM-No. 150.

References

Arz AW, Lamy F, Pätzold J, Müller PJ, Prius M (2003) Mediterranean moisture source for early to mid-Holocene humid period in the northern Red Sea. Science 300: 118–124

Bard E, Rostek F, Sonzogni C (1997) Inter-hemispheric synchrony of the last deglaciation inferred from alkenone palaeothermometry. Nature 385: 707–710

Bard E, Rostek F, Turon JL, Gendreau S (2000) Hydrological impact of Heinrich Events in the subtropical northeast Atlantic. Science 289: 1321–1324

Bard E (2001) Comparison of alkenone estimates with other paleotemperature proxies. Geochem Geophys Geosyst 2 DOI 2000GC000050

Bond G, Showers W, Cheseby M, Lotti R, Almasi P, deMenocal P, Priore P, Cullen H, Hajdas I, Bonani G (1997) A pervasive millinnial-scale cycle in North Atlantic Holocene and glacial climates. Science 278: 1257–65

Brassell SC, Eglinton G, Marlowe IT, Pflaumann U, Sarnthein M (1986) Molecular stratigraphy: a new tool for climatic assessment. Nature 320: 129–133

Cacho I, Grimalt JO, Pelejero C, Canals M, Sierro FJ, Flores JA, Shackleton NJ (1999) Dansgaard-Oeschger and Heinrich event imprints in Alboran Sea paleotemperatures. Paleoceanography 14: 698–705

Cacho I, Grimalt JO, Canals M, Sbaffi L, Shackleton NJ, Shonfeld J, Zahn R (2001) Variability of the Western Mediterranean sea surface temperatures during the last 25 000 years and its connection with the Northern Hemisphere climatic changes. Paleoceanography 16: 40–52

Calvo E, Grimalt J, Jansen E (2002) High resolution U^{K}_{37} sea surface temperature reconstruction in the Norwegian Sea during the Holocene. Quat Sci Rev 21: 1385–1394

Capotondi L, Borsetti AM, Morigi C (1999) Foraminiferal ecozones: a high resolution proxy for the late Quaternary biochronology in the central Mediterranean Sea. Mar Geol 153: 253–274

Clark PU, Pisias NG, Stocker TF, Weaver AJ (2002) The role of the thermohaline circulation in abrupt climate change. Nature 415: 863–869

Clement AC, Seager R, Cane MA (1999) Orbital controls on ENSO and the tropical climate. Paleoceanography 14: 441–456

Conte MH, Thompson A, Eglinton G, Green JC (1995) Lipid biomarker diversity in the coccolithophorid *Emiliania huxleyi* (*Prymnesiophyceae*) and the related species Gephyrocapsa oceanica. J Phycol 31: 272–282

Crowley TJ, North GR (1991) Paleoclimatology. Oxford University Press New York NY, USA

Delworth TL, Mann ME (2000) Observed and simulated multidecadal variability in the Northern Hemisphere. Clim Dyn 16: 661–676

Denton GH, Karlen W (1973) Holocene climatic variations - Their pattern and possible cause. Quat Res 3: 155–205

deMenocal P, Ortiz J, Guilderson T, Adkins J, Sarnthein M, Baker L, Yaarusinsky M (2000) Abrupt onset and termination of the African Humid Period: rapid climate responses to gradual insolation forcing. Quat Sci Rev 19: 347–361

Duplessy JC, Bard E, Arnold M, Shackleton NJ, Duprat J, Labeyrie L (1991) How fast did the ocean-atmosphere system run during the last deglaciation? Earth Planet Sci Lett 103: 27–40

Emeis KC, Struck U, Schulz HM, Rosenberg R, Bernasconi S, Erlenkeuser H, Sakamoto T, Martinez-Ruiz F (2000) Temperature and salinity variations of Mediterranean Sea surface waters over the last 16,000 years from records of planktonic stable oxygen isotopes and alkenone unsaturation ratios. Palaeogeogr Palaeoclimatol Palaeoecol 158: 259–280

Emeis KC, Schulz H, Struck U, Rossignol-Strick M, Erlenkeuser H, Howell MW, Kroon D, Mackensen A, Ishizuka S, Oba T, Sakamoto T, Koizumi I (2003) Eastern Mediterranean surface water temperatures and $\delta^{18}O$ composition during deposition of sapropels in the late Quaternary. Paleoceanography 18 DOI 10.1029/2000PA000617

Fisher H (2001) Imprint of large-scale atmospheric transport patterns on sea-salt records in northern Greenland ice cores. J Geophys Res 106: 23977–23984

Garric G, Hubber M (2003) Quasi-decadal variability in paleoclimate records: sunspont cycle or intrinsic oscillations? Paleoceanography 18:DOI 10.1029/2002PA000869

Ghil M, Allen RM, Dettinger MD, Ide K, Kondrashov D, Mann ME, Robertson A, Saunders A, Tian Y, Varadi F, Yiou P (2002) Advanced spectral methods for climatic time series. Rev Geophys 40:3.1-3.41 DOI 1029/2000GR000092

Giunta S, Emeis KC, Negri A (2001) Sea-surface temperature reconstruction of the last 16,000 years in the eastern Mediterranean Sea. Riv Ital Paleont Stratigr 107: 463–476

Goodman J, Marshall J (1999) A model of decadal middle-latitude atmosphere-ocean coupled mode. J Clim 12: 621–641

Grootes PM, Stuiver M (1997) Oxygen 18/16 variability in Greenland snow and ice with 10^{-3} to 10^{-5} year time resolution. J Geophys Res 102: 455–26470

Hagelberg T, Bond G, deMenocal P (1994) Milankovitch band forcing of sub-Milankovitch climate variability during the Pleistocene. Paleoceanography 9: 545–558

Hurrell JW, Kushnir Y, Visbeck M, Ottersen G (2003) An overview of the North Atlantic Oscillation. In: Hurrell JW, Kushnir Y, Ottersen G, Visbeck M (eds) The North Atlantic Oscillation: climate significance and environmental impact. Geophysical Monograph Series 134: 1–35

Huntley B, Prentice C (1988) July temperatures in Europe from pollen data 6000 years before present.Science 241: 687–690

James PM, James IN (1989) Ultra-low-frequency variability in a simple atmospheric circulation model. Nature 342: 53–55

Jones PD (1987) The early twentieth century Arctic High - fact or fiction? Clim Dyn 1: 63–75

Kaplan A, Cane MA, Kushnir Y, Clement AC, Blumenthal M, Rajagopalan B (1998) Analyses of global sea surface temperature 1856-1991. J Geophys Res 103: 18,567–18,589

Keigwin LD, Pickart RS (1999) Slope water current over the Laurentian Fan on interannual to millennial time scales. Science 286: 520–523

Kienast M, Steinke S, Stattegger K, Calvert SE (2001) Synchronous tropical South China Sea SST change and Greenland warming during deglaciation. Science 291: 2132–2134

Kim J-H, Schneider RR, Mulitza S, Müller PJ (2003) Reconstruction of SE trade wind intensity based on sea-surface temperature gradients in the SE Atlantic over the last 25 kyr. Geophys Res Lett 30:2144 DOI 10.1029/2003GL017557

Kim J-H, Rimbu N, Lorenz SJ, Lohmann G, Nam S-I, Schouten S, Rühlemann C, Schneider RR (2004) North Pacific and North Atlantic sea-surface temperature variability during the Holocene. Quat Sci Rev (accepted)

Kitoh A, Murakami S (2002) Tropical Pacific climate at the mid-Holocene and the Last Glacial Maximum simulated by a coupled ocean-atmosphere general circulation model. Paleooceanography 17:DOI 10.1029/2001PA000724

Latif M, Barnett TP (1994) Causes of decadal climate variability over the North Pacific and North America. Science 266: 634–637

Legutke S, Voss R (1999) The Hamburg atmosphere-ocean coupled circulation model ECHO-G. Deutsches Klimarechenzentrum Hamburg Techn Rep 18, Hamburg, Germany

Lohmann G, Lorenz S, Prange M (2004) Northern high-latitude climate changes during the Holocene as simulated by circulation models. AGU Monographs, Bjerknes book about the Nordic Seas (accepted)

Lorenz SJ, Lohmann G (2004) Acceleration technique for Milankovitch type forcing in a coupled atmosphere-ocean circulation model. Cim Dyn (accepted)

Marchal O, Cacho I, Stocker TF, Grimalt JO, Calvo E, Martrat B, Shackleton N, Vautravers M, Cortijo E, van Kreveld S, Andersson C, Koc N, Chapman M, Sbaffi L, Duplessy JC, Sarnthein M, Turon JL, Duprat J, Jansen E (2002) Apparent long-term cooling of the sea surface in the Northeast Atlantic and Mediterranean during the Holocene. Quat Sci Rev 21: 455–483

Mayewski PA, Meeker LD, Twickler MS, Whitlow S, Yang Q, Lyons WB, Prentice M (1997) Major features and forcing of high-latitude Northern Hemisphere atmospheric circulation using a 110 000 year-long glaciochemical series. J Geophys Res 102: 26 345–65

Müller PJ, Kirst G, Ruhland G, von Storch H, Rosell-MeléA (1998) Calibration of the alkenone palaeotemperature index $U_{37}^{K'}$ based on core-tops from the eastern South Atlantic and the global ocean (60°N–60°S). Geochim Cosmochim Acta 62: 1757–1772

Noren JA, Bierman PR, Steig JE, Lini A, Southon J (2002) Millenial-scale storminess variability in the northeastern United States during the Holocene epoch. Nature 419: 821–824

O'Brien SR, Mayewski PA, Meeker LD, Meese DA, Twinckler MS, Whitlow SI (1995) Complexity of Holocene climate as reconstructed from Greenland ice core. Science 270: 1962–1964

Pelejero C, Grimalt JO (1997) The correlation between the U^{K}_{37} index and sea surface temperatures in the warm boundary: the South China Sea. Geochim Cosmochim Acta 61: 4789–4797

Pelejero C, Grimalt JO, Heilig S, Kienast M, Wang L (1999a) High-resolution $U_{37}^{K'}$ temperature reconstructions in the South China Sea over the past 220 kyr. Paleoceanography 14: 224–231

Pelejero C, Kienast M, Wang L, Grimalt JO (1999b) The flooding of Sundaland during the last deglaciation: imprints in hemipelagic sediments from the southern South China Sea. Earth Planet Sci Lett 171: 661–671

Pestiaux P, van der Mersch I, Berger A, Duplessy JC (1988) Paleoclimatic variabiity at frequencies ranging from 1/10000 to 1/1000 years; evidence for nonlinear behaviour in the climate system. Clim Change 12: 9–37

Porter SC, Orombelli G (1985) Glacier contraction during the middle Holocene in the western Italian Alps: evidence and implications. Geology 13: 296–298

Prahl FG, Wakeham SG (1987) Calibration of unsaturation patterns in long-chain ketone compositions for paleotemperature assessment. Nature 330: 367–369

Prahl FG, Muehlhausen LA, Zahnle DL (1988) Further evaluation of long-chain alkenones as indicators of paleoceanographic conditions. Geochim Cosmochim Acta 52: 2303–2310

Pozo-Vázquez D, Esteban-Parra MJ, Rodrigo FS, Castro-Diez Y (2001) The association between ENSO and winter atmospheric circulation and temperature in the North Atlantic region. J Clim 14: 3408–3420

Rimbu N, Lohmann G, Felis T, Pätzold J (2001) Arctic Oscillation signature in a Red Sea coral. Geophys Res Lett 28: 2959–2962

Rimbu N, Lohmann G, Kim J-H, Arz HW, Schneider RR (2003) Arctic/North Atlantic Oscillation signature in Holocene sea surface temperature trends as obtained from alkenone data. Geophys Res Lett 30: DOI 10.1029/2002GL016570

Rodbell DT, Seltzer GO, Anderson DM, Abbott MB, Enfield DB, Newman JH (1999) A 15,000 -year record of El Niño alluviation in southwestern Ecuador. Science 283: 516–520

Rohling EJ, Mayewski PA, Hayes A, Abu-Zied RH, Casford JSL (2002) Holocene atmosphere-ocean interactions: records from Greenland and the Aegean Sea. Clim Dyn 18: 573–592

Rosell-Melé A, Eglinton G, Pflaumann U, Sarnthein M (1995) Atlantic core-top calibration of the $U^{K'}_{37}$ index as a sea-surface palaeotemperature indicator. Geochim Cosmochim Acta 59: 3099–3107

Rühlemann C, Mulitza S, Müller PJ, Wefer G, Zahn R (1999) Warming of the tropical Atlantic Ocean and slowdown of thermohaline circulation during the last deglaciation. Nature 402: 511–514

Sarnthein M, van Kreveld S, Erlenkeuser H, Grootes PM, Kucera M, Pflaumann U, Schulz M (2003) Centennial-to-millennial-scale periodicities of Holocene climate and sediment injections off the western Barents shelf, 75°N. Boreas 32: 447–461

Schulz M, Paul A (2002) Holocene climate variability on centennial-to-millennial time scales: 1. Climate records from the North-Atlantic realm. In: Wefer G, Berger WH, Behre KE, Jansen E (eds.) Climate development and history of the North Atlantic Realm. Springer Heidelberg New York Berlin pp 41–54

Shindell DT, Schmidt GA, Miller RL, Mann ME (2003) Volcanic and solar forcing of climate change during the preindustrial era. J Clim 16: 4094–4107

Shindell DT, Schmidt GA, Mann ME, Rind D, Waple A (2001) Solar forcing of regional climate change during the Maunder Minimum. Science 294: 2149–2152

Siani G, Paterne M, Michel E, Sulpizio R, Sbrana A, Arnold M, Haddad G (2001) Mediterranean sea-surface radiocarbon reservoir age changes since the last glacial maximum. Science 294: 1917–1920

Sirocko F, Sarnthein M, Erlenkeuser H, Lange H, Arnold M, Duplessy JC (1993) Century-scale events in monsoonal climate over the past 24,000 years. Nature 364: 322–324

Sonzogni C, Bard E, Rostek F (1998) Tropical sea surface temperatures during the last glacial period: a view based on alkenones in Indian Ocean sediments. Quat Sci Rev 17: 1185–1201

Thompson DWJ, Wallace JW (1998) The Arctic Oscillation signature in the wintertime geopotential height and temperature fields. Geophys Res Lett 25: 1297–1300

Tudhope AW, Chilcott CP, McCulloch MT, Cook ER, Chappell J, Ellam RM, Lea DW, Lough JM, Shimmield GB (2001) Variability in the El Niño-Southern Oscillation through a glacial-interglacial cycle. Sci 291: 1511–1517

von Storch H, Zwiers FW (1999) Statistical analysis in climate research. Cambridge University Press, Cambridge UK pp 735

Volkman JK, Eglinton G, Corner EDS, Sargent JR (1980) Novel unsaturated straight-chain methyl and ethyl ketones in marine sedimens and a coccolithophore *Emiliania huxleyi*. In: Douglas AG, Maxwell JR (eds) Advances in Organic geochemistry. Pergamon, Tarrytown NY, USA pp 219–227

Wang L, Sarnthein M, Erlenkeuser H, Heilig S, Ivanova E, Kienast M, Pflaumann U, Pelejero C, Grootes P (1999) East Asian monsoon during the late Quaternary: high-resolution sediment records from the South China Sea. Mar Geol 156: 245–284

Zebiak SE, Cane MA (1987) A model for El Niõ- Southern Oscillation. Mon Wea Rev 115: 2262–2278

Zhao M, Beveridge NAS, Shackleton NJ, Sarnthein M, Eglinton G (1995) Molecular stratigraphy of cores off northwest Africa: Sea surface temperature history over the last 80 ka. Paleoceanography 10: 661–675

Zhang HC, Ma YZ, Wunneman B, Pachur HZ (2000) A Holocene climatic record from arid northwestern China. Paleogeogr Paleoclimatol Paleoecol 162: 389–401